

# Spatial Peak-Aware Collaborative Representation for Hyperspectral Imagery Classification

Chengle Zhou<sup>1</sup>, Graduate Student Member, IEEE, Bing Tu<sup>1</sup>, Member, IEEE,  
Qi Ren, Student Member, IEEE, and Siyuan Chen

**Abstract**—In this letter, a novel spatial peak-aware collaborative representation (SPaCR) method is proposed for hyperspectral imagery (HSI) classification, which introduces spectral-spatial information among superpixel clusters into regularization terms to construct a new collaborative representation (CR)-based closed-form solution. The proposed method is composed of the following key steps. First, the raw HSI is clustered into many superpixels according to an oversegmentation strategy. Then, cluster pixels are determined based on spectral-spatial correlation between pixels within each superpixel. Next, spectral distance and spatial coherence of superpixel clusters corresponding to training samples and testing pixels are fused to define differences between pixels. Finally, the difference information between clusters as a spectral-spatial feature-induced regularization term is incorporated into the objective function. Experimental results on the Indian Pines and the University of Pavia HSIs indicated that the proposed SPaCR method, without any preprocessing and postprocessing, outperforms well-known and state-of-the-art classifiers on the limited labeled samples.

**Index Terms**—Collaborative representation (CR), hyperspectral imagery (HSI), spatial peak regularization, spectral-spatial classification, superpixel.

## I. INTRODUCTION

**H**YPERSPECTRAL imagery (HSI) can capture the characteristics of ground coverings in remotely sensed scenes via hundreds of narrow and continuous spectrum bands, and

Manuscript received January 1, 2021; revised April 16, 2021; accepted May 20, 2021. This work was supported in part by the National Natural Science Foundation of China under Grant 61977022; in part by the Science Foundation for Distinguished Young Scholars of Hunan Province under Grant 2020JJ2017; in part by the Natural Science Foundation of Hunan Province under Grant 2019JJ50211, Grant 2019JJ50212, Grant 2020JJ4340, and Grant 2020JJ4343; in part by the Key Research and Development Program of Hunan Province under Grant 2019SK2102; in part by the Foundation of Education Bureau of Hunan Province under Grant 19B245, Grant 19B237, and Grant 20B257; in part by the Engineering Research Center on 3-D Reconstruction and Intelligent Application Technology of Hunan Province under Grant 2019-430602-73-03-006049; in part by the Hunan Emergency Communication Engineering Technology Research Center under Grant 2018TP2022; and in part by the Guangxi Key Laboratory of Cryptography and Information Security under Grant GCIS201911. (Corresponding author: Bing Tu.)

Chengle Zhou, Qi Ren, and Siyuan Chen are with the School of Information Science and Engineering, Hunan Institute of Science and Technology, Yueyang 414000, China (e-mail: chengle\_zhou@foxmail.com; ren\_qi1113@foxmail.com; siyuan@hnist.edu.cn).

Bing Tu is with the School of Information Science and Engineering, Hunan Institute of Science and Technology, Yueyang 414000, China, and also with the Guangxi Key Laboratory of Cryptography and Information Security, Guilin University of Electronic Technology, Guilin 541000, China (e-mail: tubing@hnist.edu.cn).

Color versions of one or more figures in this letter are available at <https://doi.org/10.1109/LGRS.2021.3083416>.

Digital Object Identifier 10.1109/LGRS.2021.3083416

thus, the development of well-suited technologies for variedly remote-sensing applications has attracted the interest of researchers, such as classification [1], [2].

Over the years, a lot of collaborative representation (CR)-based supervised learning algorithms have been successfully introduced into HSIs classification, which effectively solves the problem of ground cover identification and classification at the pixelwise level [3]–[9]. Li *et al.* [3] and Li and Du [4] proposed advanced CRCs by designing  $l_2$ -norm minimization-derived closed-form solution to estimate representation weight and introducing spatial mean feature constrained by the fixed window into the spectral feature of samples, respectively. Moreover, driven by the feasibility of kernel tricks in the HSI, Li *et al.* [5] presented a kernel CR with Tikhonov regularization (KCRT), and Ma *et al.* [6] developed a discriminative kernel CR and a Tikhonov regularization method (DKCRT). The above-mentioned two KCR-based classifiers aim to employ the kernel trick to promote the spectral separability of pixels, so as to improve the classification accuracy of the CR model.

Differing from the above approaches, Jiang *et al.* [7] defined a classifier via spatial-aware collaborative representation (SaCR); the key technology behind their work is that the spatial and spectral features are both utilized to generate the distance-weighted regularization terms. In [8], a structure-aware CR with the Tikhonov regularization (SaCRT) method is proposed to consider both label information of training samples and spectral signatures of testing pixels to estimate more discriminative representation coefficients. Furthermore, Karaca [9] presented a classifier by embedding domain transform filter (DTF) into the processing of SaCR; experimental results proved the method can achieve good classification performance at limited labeled data.

However, these CR-based methods fail to consider the spectral-spatial information among superpixel clusters. In fact, the clusters carry numerous interesting information that can smooth salt-pepper noise in the final result and improve the classification accuracy of the CRC. Inspired by this, this letter develops a novel spatial peak-aware collaborative representation (SPaCR) method for HSI classification, which directly introduces spectral-spatial information among superpixel clusters into regularization terms to construct a new CR-based closed-form solution. Specifically, experimental results on two HSI benchmark datasets indicated that the proposed method without any preprocessing and postprocessing can achieve promising classification accuracy even with a very limited number of training data with respect to several well-known and state-of-the-art classifiers.

## II. RELATED WORK

### A. CR in HSI Classification

Assume that hyperspectral data  $\mathbf{D}$  are divided into the training set  $\mathbf{X} = \{\mathbf{X}_1, \mathbf{X}_2, \dots, \mathbf{X}_c\} \in \mathbb{R}^{m \times n}$  and the testing set  $\mathbf{Y}$ ,  $c$  is the number of class,  $m$  refers to spectral dimension of a sample,  $n$  represents the total number of training sample, and  $\mathbf{X}_i = \{\mathbf{x}_{i1}, \mathbf{x}_{i2}, \dots, \mathbf{x}_{in_i}\} \in \mathbb{R}^{m \times n_i}$  is a subdictionary, which is composed of  $n_i$  samples from the  $i$ th class. According to the CR rule, a test pixel belonging to  $i$ th class can be represented as

$$\mathbf{y} \approx \sum_{j=1}^{n_i} \mathbf{x}_{ij} \alpha_{ij} \quad (1)$$

where  $\alpha_{ij}$  is a representation coefficient (weight) corresponding sample  $\mathbf{x}_{ij}$  in subdictionary  $\mathbf{X}_i$ .

If the dictionary consists of all training samples, then the test pixel  $\mathbf{y} \in \mathbb{R}^m$  can be expressed as

$$\mathbf{y} = \hat{\mathbf{y}} + \mathbf{e} = \sum_{i=1}^c \sum_{j=1}^{n_i} \mathbf{x}_{ij} \alpha_{ij} + \mathbf{e} \approx \sum_{i=1}^c \sum_{j=1}^{n_i} \mathbf{x}_{ij} \alpha_{ij} = \mathbf{X} \boldsymbol{\alpha} \quad (2)$$

where  $\mathbf{e}$  refers to residual generated by noise. Thus, the weight vector  $\boldsymbol{\alpha}$  can be obtained by solving a constrained optimization problem, as follows:

$$\boldsymbol{\alpha}^* = \arg \min_{\boldsymbol{\alpha}} \|\boldsymbol{\alpha}\|_2^2. \quad (3)$$

Meanwhile, there is the following relationship:

$$\|\mathbf{y} - \mathbf{X} \boldsymbol{\alpha}\| \leq \varepsilon \quad (4)$$

where  $\varepsilon$  represents an error constraint. Then, we can use the Lagrangian equation to transform the above problem as

$$\boldsymbol{\alpha}^* = \arg \min_{\boldsymbol{\alpha}} \|\mathbf{y} - \mathbf{X} \boldsymbol{\alpha}\|_2^2 + \lambda \|\boldsymbol{\alpha}\|_2^2 \quad (5)$$

where  $\lambda$  is a regularization parameter, which can be utilized to balance relationship between reconstruction residual and regularization term. Once the optimal weighted coefficient is obtained, the label of the test sample can finally be determined by the following expression:

$$\text{Class}(\mathbf{y}) = \arg \min_{i=1,2,\dots,c} \|\mathbf{y} - \mathbf{X}_i \boldsymbol{\alpha}_i^*\|_2^2. \quad (6)$$

Besides, to make the representation more flexible, Li *et al.* [3] proposed a nearest regularized CR model, which introduces a regular term of locality constraint into the solution (5) by granting various freedom to training samples based on their Euclidean distances from  $\mathbf{y}$

$$\boldsymbol{\alpha}^* = \arg \min_{\boldsymbol{\alpha}} \|\mathbf{y} - \mathbf{X} \boldsymbol{\alpha}\|_2^2 + \lambda \|\boldsymbol{\alpha}\|_2^2 \quad (7)$$

where  $\boldsymbol{\Gamma}$  refers to a biasing Tikhonov matrix defined by  $\boldsymbol{\Gamma}_i = \|\mathbf{y} - \mathbf{X}_i\|_2$ . If the distance between a training sample  $\mathbf{x}_i$  and the test pixel  $\mathbf{y}$  is large,  $\mathbf{x}_i$  will be given a small representation coefficient  $\alpha_i$ , and vice versa.

To take into consideration the spatial information of HSI, Li and Du [4] presented a joint CR model, which use spatial average strategy to represent each sample, as follows:

$$\boldsymbol{\alpha}^* = \arg \min_{\boldsymbol{\alpha}} \|\bar{\mathbf{y}} - \mathbf{X} \bar{\mathbf{X}} \boldsymbol{\alpha}\|_2^2 + \lambda \|\boldsymbol{\alpha}\|_2^2 \quad (8)$$

where  $\bar{\mathbf{y}}$  represents the average spectral value of pixels in the spatial window centered on  $\mathbf{y}$  and  $\bar{\mathbf{X}}$  represents the new

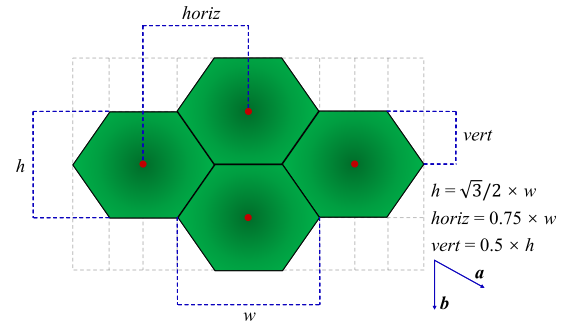


Fig. 1. Metrics of flat-topped hexagonal grids.

dictionary formed by each pixel in the  $\mathbf{X}$  after all pixels in the spatial window centered on it are averaged.

Unlike the above CR models, Jiang *et al.* [7] merged the spatial coordinate of pixels into objective function (7) by designing a spatial regularization term

$$\boldsymbol{\alpha}^* = \arg \min_{\boldsymbol{\alpha}} \|\mathbf{y} - \mathbf{X} \boldsymbol{\alpha}\|_2^2 + \lambda \|\boldsymbol{\Gamma} \boldsymbol{\alpha}\|_2^2 + \gamma \|\text{diag}(\mathbf{s}) \mathbf{a}\|_2^2 \quad (9)$$

where  $\mathbf{s}$  is associated with training samples, which encourages representation coefficients that are spatially coherent with respect to the training sample, and  $\text{diag}(\mathbf{s})$  returns a diagonal matrix with the elements of vector  $\mathbf{s}$  on the main diagonal.

### B. HSI Oversegmentation

Oversegmentation technology has been widely used in the HSI classification due to its powerful spatial neighborhood definition ability, such as simple linear iterative clustering (SLIC) [10], entropy rate superpixel (ERS) [11], and gradient ascent-based SLIC (GA-SLIC) [12]. For the later, superpixels associate with clusters in the defined spectral-spatial space. Meanwhile, to improve the homogeneity of each cluster, regular hexagonal grids are employed to generate the initial clusters, instead of the square grids used in the SLIC. As shown in Fig. 1, the size of the hexagons can be represented by the width  $w$  and height  $h$ , and the spacing among adjacent hexagons can be described by the horizontal distance  $\text{horiz}$  and the vertical distance  $\text{vert}$ . The face centers of hexagons can be defined as a simple matrix multiplication

$$\begin{bmatrix} C_x(t) \\ C_y(t) \end{bmatrix} = \begin{bmatrix} \text{horiz} & 0 \\ \text{vert} & h \end{bmatrix} \begin{bmatrix} \text{row}_t \\ \text{col}_t \end{bmatrix} \quad (10)$$

where  $[\text{row}_t, \text{col}_t]^T$  refers to the row and column indexes of the  $t$ th superpixel, and vectors  $\mathbf{a} = [\text{horiz}_t, \text{vert}_t]^T$  and  $\mathbf{b} = [0_t, h_t]^T$  consist of the hexagonal coordinates, for which the origin is at the upper left of the image. Note that more details of the GA-SLIC can be found in [12].

## III. PROPOSED APPROACH

### A. Motivation

Existing CR models either expand adjacent pixels to introduce a spatial feature or obtain spatial information by averaging the spectral features of neighboring pixels. However, these models often show low classification accuracy and many salt-pepper noises in the final results. Inspired by this, we merged spatial information into the objective function by adding a regular term induced by the superpixel cluster (see Fig. 2) to improve the performance of the CR model.

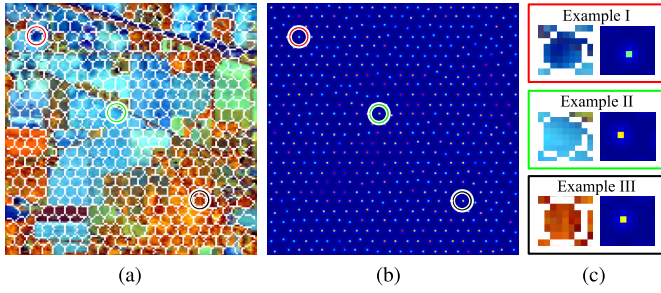


Fig. 2. Illustration of GA-SLIC-based segmentation image on the Indian Pines image. (a) Superpixel block. (b) Corresponding cluster. (c) Local view.

### B. Contribution

For the proposed SPaCR method, the main innovative contributions can be summarized as follows.

- 1) We introduce spectral-spatial information of superpixel clusters in the pixel-level CR paradigm and incorporate that into objective function by designing a spatial feature-induced regularization term for the first time.
- 2) In comparing classic and advanced classifiers, it is found that the SPaCR classifier on the limited labeled data can achieve outstanding accuracy without any preprocessing and postprocessing.

In the following, we will describe the proposed SPaCR method for HSI classification in detail.

### C. SPaCR

In this section, the three key steps of the proposed SPaCR method<sup>1</sup> are clearly presented as follows.

1) *Oversegmentation-Based Pixel Clustering*: In our model, assume that  $I_s$  refers to the segmentation details corresponding to  $S_n$  superpixel blocks, and  $C = [C_1, C_2, \dots, C_{S_n}]$  is the cluster center of all of superpixel.  $D \in \mathbb{R}^m$  as an input can be first fed into the GA-SLIC algorithm to generate superpixel blocks with hexagon and cluster pixels, which can be simply represented as follows:

$$(I_s, C) = \text{GA-SLIC}(D, S_w, \omega_s) \quad (11)$$

where  $S_w$  is the average width of superpixels and  $\omega_s$  is tradeoff coefficient between spatial and spectral information that be employed to update cluster. Then, the cluster center of the  $t$ th superpixel is detailedly expressed as follows:

$$C_t = [r_1^t, r_2^t, \dots, r_m^t, C_x(t), C_y(t)]^T \in \mathbb{R}^{m+2} \quad (12)$$

where  $\bar{r}^t = [r_1^t, r_2^t, \dots, r_m^t]^T$  is the mean spectral reflectance of the  $t$ th superpixel, and  $[C_x(t), C_y(t)]$  refers to the spatial coordinates of the  $t$ th cluster pixel.

2) *Superpixel-Based Spectral-Spatial Distance*: Suppose that  $x_i^t$  is a training sample located in the  $t$ th superpixel from the  $i$ th class, and  $y^k$  is a test sample belonging to the  $k$ th superpixel. The superpixel spectral-spatial distance  $d_i$  between  $x_i^t$  and  $y^k$  can be defined as follows:

$$d_{\text{SAM}}^i(t, k) = \arccos\left(\frac{\bar{r}(x_i^t)^T \bar{r}(y^k)}{\|\bar{r}(x_i^t)\|_2 \|\bar{r}(y^k)\|_2}\right) \quad (13)$$

$$d_{\text{Ed}}^i(t, k) = \sqrt{\{C_x(t) - C_x(k)\}^2 + \{C_y(t) - C_y(k)\}^2} \quad (14)$$

<sup>1</sup>MATLAB demo is available online at [github.com/chengle-zhou](https://github.com/chengle-zhou).

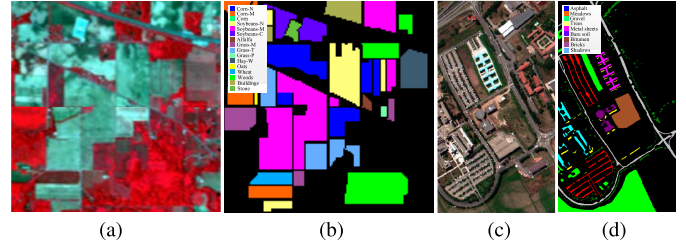


Fig. 3. False-color composites and corresponding reference data for different datasets. (a) and (b) Indian Pines image. (c) and (d) University of Pavia image.

$$d_i = \sqrt{\text{norm}(d_{\text{SAM}}^i(t, k)^2) + \text{norm}(d_{\text{Ed}}^i(t, k)^2)} \quad (15)$$

where  $\bar{r}(\cdot)$  represents the mean spectral feature of superpixel,  $\text{norm}(\cdot)$  is denoted as the  $L_2$ -norm normalization operation, and  $C_x(\cdot)$  ( $C_y(\cdot)$ ) refers to the row (column) coordinate of the cluster pixel of the corresponding superpixel.  $d_{\text{SAM}}^i(t, k)$  and  $d_{\text{Ed}}^i(t, k)$  are spectral and spatial distances between training sample (located in the  $t$ th superpixel) and test pixel (located in  $k$ th superpixel), respectively.

3) *Superpixel-Based Spatial Peak Regularization*: Once obtaining the  $\mathbf{d} = [d_1, d_2, \dots, d_c]$ , superpixel cluster information as a regularization can be directly incorporated into objective function

$$\alpha^* = \arg \min_{\alpha} \|\mathbf{y} - \mathbf{X}\alpha\|_2^2 + \lambda \|\mathbf{\Gamma}\alpha\|_2^2 + \beta \|\Lambda(\mathbf{d})\alpha\|_2^2 \quad (16)$$

where  $\lambda$  and  $\beta$  are adjustable free parameters that control the contributions of the locality prior (second term) and cluster prior (third term), respectively. The role of  $\Lambda(\mathbf{d})$  in (16) is similar to that of  $\mathbf{\Gamma}$ , in which the closer the test sample is to the training sample, the smaller the  $d_i$ , and vice versa. Finally, the optimization process of (16) is analogous to (7), which is derived analytically as follows:

$$\alpha^* = (\mathbf{x}^T \mathbf{X} + \lambda \mathbf{\Gamma} + \beta \Lambda(\mathbf{d})) \mathbf{x}^T \mathbf{y}. \quad (17)$$

## IV. EXPERIMENTAL RESULTS

### A. Experimental Setup

To test the classification performance of the proposed SPaCR method, several experiments are performed on two real HSI datasets: Indian Pines and the University of Pavia. The first dataset is composed of 220 spectral bands across the spectral range of 0.4–2.5  $\mu\text{m}$ , and each band contains  $145 \times 145$  pixels with a spatial resolution of 20 m/pixel. In our experiments, 20 water absorption bands (nos. 140–108, 150–163, and 220) of these data were removed. The second dataset is of size  $610 \times 340 \times 120$  with a spatial resolution of 1.3 m/pixel and a spectral coverage in the range 0.43–0.86  $\mu\text{m}$ ; 12 spectral bands were removed before the classification due to high noise. Fig. 3(a)–(d) shows the false-color composites and their corresponding reference data for different datasets. It is worth noting that, for the two datasets, the number of training samples trained by all classifiers in this letter, respectively, accounts for 1.0% and 0.42% of the labeled data. Furthermore, three objective metrics, i.e., overall accuracy (OA), average accuracy (AA), and the Kappa coefficient, are employed in our follow-up experiments to judge classification advantage between competitive methods and the SPaCR method.



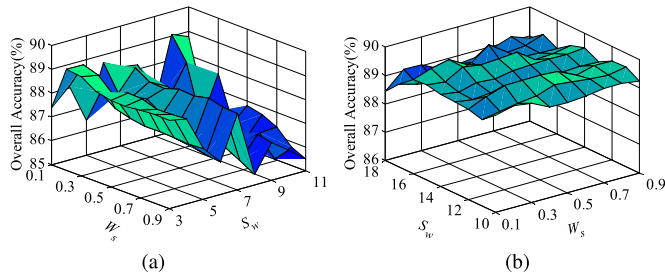


Fig. 4. Analysis of the influence of the parameters  $S_w$  and  $W_s$  on the classification performance of the SPaCR for the different scenes. (a) Indian Pines dataset. (b) University of Pavia dataset.

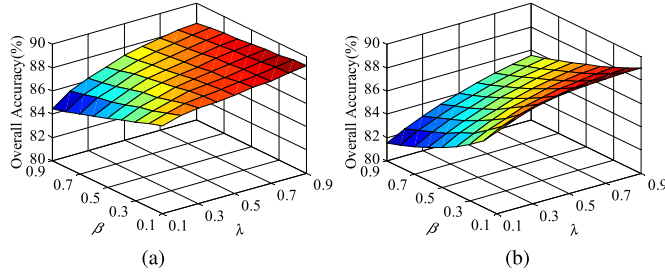


Fig. 5. Influence of the regularization parameters on classification accuracies with various values of  $\lambda$  and  $\beta$ . (a) Indian Pines dataset. (b) University of Pavia dataset.

### B. Parameter Settings

In this section, the influence of the crucial parameters on the proposed method is analyzed in the above two real scenes. These parameters are the average width of superpixel  $S_w$ , tradeoff coefficient  $\omega_s$  between spatial and spectral distance, and the regularization parameters  $\lambda$  and  $\beta$ .

In the first experiment, we analyze the impact of the parameters  $S_w$  and  $\omega_s$  on the classification performance of the SPaCR method. As shown in Fig. 4, it can be significantly observed that OAs first rises and then falls as the variousness of  $S_w$  when  $\omega_s$  is fixed. This means that the size of the superpixel will directly affect the determination of the cluster center and, thus, the accuracy of the SPaCR. When  $S_w$  is fixed, the fluctuation trend of OA does not change significantly with  $\omega_s$ . The reason is that the cluster position mainly depends on the superpixel size, and the spectral-spatial distance between the pixels in the superpixel is just to make its position more accurate. Furthermore, we conduct the second experiment to dissect the influence of  $\lambda$  and  $\beta$  on the performance of the SPaCR method. The range of  $\lambda$  and  $\beta$  is set to 0.1–0.9, respectively. In Fig. 5, it can be seen that OAs showed a steady upward trend as  $\beta$  gradually increased in the interval of 0.1–0.9 when  $\lambda$  is taken a fixed value. It is demonstrated that the CR-based classifier can be effectively improved with the introduction of superpixel-based spatial peak regularization terms in terms of classification accuracy (especially when it occupies a large proportion). Finally, according to the experimental results on real HSI datasets, the optimal parameters on the SPaCR method are presented in Table I. In addition, we suggest that the expansion of the SPaCR to new datasets requires the proper adjustment of the abovementioned important parameters.

### C. Spatial Advantages of Superpixel Cluster

Here, spatial advantages of superpixel cluster with respect to pixel in terms of the measure of spatial coherence are analyzed on the abovementioned datasets. Training samples in the two datasets trained by the SaCR and SPaCR methods are account

TABLE I  
PARAMETER SETTINGS OF THE PROPOSED SPaCR METHOD FOR THE TWO HSI DATASETS

Datasets	Crucial parameters			
	$S_w$	$\omega_s$	$\lambda$	$\beta$
Indian Pines	3	0.2	0.2	0.4
University of Pavia	12	0.5	0.1	0.7

TABLE II  
CLASSIFICATION ACCURACIES (IN %) OF THE SaCR AND SPaCR METHODS ON THE INDIAN PINES AND UNIVERSITY OF PAVIA DATASETS

Methods	Indian Pines		University of Pavia	
	SaCR	SPaCR	SaCR	SPaCR
OA	64.29(1.21)	85.45(1.98)	74.47(2.64)	90.73(2.37)
AA	65.47(1.52)	88.13(1.96)	80.20(1.65)	94.11(0.83)
Kappa	58.39(1.41)	83.33(2.29)	67.68(3.15)	87.98(2.93)

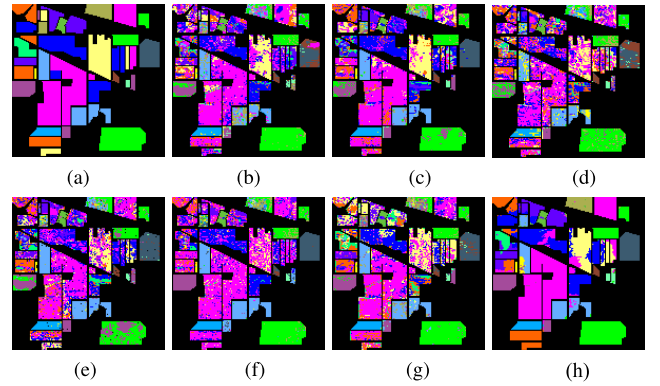


Fig. 6. Reference data and classification results (%) for the Indian Pines dataset. (a) Reference data. (b)–(h) Classification maps generated by different methods: SVM, ELM, SRC, CRC, JSaCR, SaCRT, and SPaCR.

for 1.0% and 0.42% of labeled data, respectively. We emphasize that the SaCR just considers the spatial correlation of pixel coordinate in the second regularization term of CR model [see (9)]; the SPaCR exploits both spectral-spatial distance among clusters and the cluster coordinate feature in terms of spatial correlation [see (13)–(16)]. In Table II, it can be seen that the SPaCR significantly outperforms the SaCR method in terms of OA, AA, and Kappa. The reason is that: 1) the cluster coordinate contains a more accurate spatial correlation with respect to pixel coordinate and 2) the spectral-spatial distance can weaken the deviation of coordinate information.

### D. Comparisons With Other Classifiers

In this section, the proposed SPaCR method is compared with the several well-known classifiers, i.e., the support vector machine (SVM) [13], the extreme learning machine (ELM) [14], the sparse representation classifier (SRC) [15], and CRC [3], and two state-of-the-art classifiers, i.e., joint-SaCR (JSaCR) [7] and SaCRT [8] on the abovementioned public HSI datasets. The comparison results are given in Figs. 6 and 7 and Table III, which can be clearly found following interesting phenomena as follows.

- 1) In Fig. 6, the classification result map obtained by the SPaCR has significantly less salt-pepper noise, which is closer to the reference data [see Fig. 3(b)].
- 2) In Table III, the SPaCR not only achieved the highest results in the three objective metrics but also obtained the best classification accuracies in most classes. It is

TABLE III

CLASSIFICATION ACCURACY (IN PERCENT) OF THE INDIAN PINES DATASET IN THE SVM, ELM, SRC, CRC, JSaCR, SaCRT, AND SPaCR METHODS. THE NUMBER IN THE PARENTHESIS IS THE STANDARD VARIATION OF THE ACCURACIES OBTAINED IN REPEATED EXPERIMENTS

The number of training samples is 1.0% of the reference data.									
Class	Train	Test	SVM	ELM	SRC	CRC	JSaCR	SaCRT	SPaCR
Alfalfa	3	43	22.00(6.42)	46.97(17.4)	62.09(24.1)	81.16(7.94)	69.77(13.2)	81.86(15.4)	<b>100.0(0.00)</b>
Core-N	13	1415	51.86(7.15)	57.77(5.18)	37.39(7.44)	44.27(7.40)	57.09(7.10)	61.43(4.88)	<b>75.31(6.63)</b>
Corn-M	9	821	47.28(10.5)	48.00(9.37)	36.71(7.05)	41.35(4.12)	32.57(7.00)	39.20(13.6)	<b>74.56(8.53)</b>
Corn	3	234	37.29(9.11)	44.50(16.8)	24.32(6.28)	24.36(5.06)	17.18(9.00)	44.62(17.3)	<b>76.58(14.9)</b>
Grass-M	5	478	77.49(10.9)	75.89(11.5)	57.72(9.14)	73.39(7.95)	64.18(14.4)	81.88(12.5)	<b>82.32(8.53)</b>
Grass-T	6	724	77.34(3.86)	83.75(5.47)	74.85(7.85)	81.34(11.1)	<b>96.42(1.62)</b>	88.12(6.53)	82.57(8.47)
Grass-P-M	3	25	40.44(17.1)	31.72(22.1)	84.40(11.7)	86.00(4.71)	76.00(11.2)	86.40(10.8)	<b>98.00(2.11)</b>
Hay-W	5	473	89.51(7.45)	96.96(1.16)	73.57(15.7)	88.10(7.40)	96.09(4.57)	84.74(7.07)	<b>100.0(0.00)</b>
Oats	3	17	20.25(6.57)	19.84(4.43)	71.18(18.1)	81.76(16.7)	87.65(8.52)	91.76(12.9)	<b>100.0(0.00)</b>
Soybean-N	8	964	50.42(7.12)	57.87(7.57)	40.88(7.17)	45.81(7.12)	26.43(4.91)	41.20(9.56)	<b>73.00(3.71)</b>
Soybean-M	25	2430	57.51(3.93)	60.67(3.30)	61.89(4.23)	63.59(4.74)	77.91(4.38)	67.98(3.38)	<b>96.12(2.41)</b>
Soybean-C	6	587	36.35(7.95)	54.76(11.9)	23.17(5.25)	36.85(10.1)	31.65(6.46)	55.13(16.9)	<b>69.15(9.50)</b>
Wheat	3	202	80.37(4.88)	84.43(5.40)	81.19(19.1)	98.32(1.10)	99.50(0.00)	97.52(1.26)	<b>99.60(0.21)</b>
Woods	11	1254	87.41(3.34)	87.81(5.57)	81.36(8.16)	88.41(6.67)	94.18(3.47)	93.17(1.74)	<b>98.24(3.68)</b>
Buildings	4	382	34.11(8.26)	63.26(22.0)	18.69(6.49)	24.50(5.94)	33.30(10.7)	45.45(12.8)	<b>91.07(10.3)</b>
Stone	3	90	93.12(17.7)	<b>98.13(4.53)</b>	89.56(4.69)	91.44(4.19)	92.11(4.52)	85.56(2.08)	95.78(3.95)
OA (in %)			59.44(1.48)	65.36(2.37)	54.08(1.77)	60.52(1.78)	64.75(1.55)	66.94(3.17)	<b>85.99(1.61)</b>
AA (in %)			56.42(2.00)	63.27(2.96)	57.44(1.97)	65.67(1.78)	65.75(2.56)	71.63(2.58)	<b>88.27(1.58)</b>
Kappa (in %)			53.33(1.73)	60.13(2.63)	47.54(2.00)	54.90(2.01)	58.94(1.78)	62.43(3.62)	<b>83.97(1.85)</b>

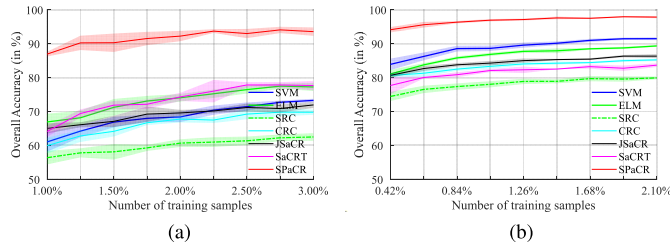


Fig. 7. Classification performance of the proposed SPaCR method with different numbers of training samples on various images. (a) Indian Pines image. (b) University of Pavia image.

worth noting that the highest accuracy of the Grass-T and Stone classes is obtained by the JSaCR and ELM methods, respectively. The reason is that the former employs a mean filter preprocessing operation before classification, and the latter belongs to a single-layer neural network, which is more sensitive to the spectral properties of the Stone class than the CR model.

3) In Fig. 7, the SPaCR method can still maintain absolute classification advantages as the number of training samples increases on the two HSI datasets.

In summary, this means that it is effective to introduce the spatial peak regularization term into the CR model, and it also proves the practicability of the SPaCR for HSI classification.

## V. CONCLUSION

In this letter, a novel SPaCR method has been introduced for HSI classification, which incorporates spectral-spatial information among superpixel clusters into regularization terms to construct a new CR-based closed-form solution. Specifically, the difference information (i.e., spectrum and coordinate) between clusters corresponding to training and test pixels as a spectral-spatial feature-induced regularization term is directly merged into the objective function. Experiments on several benchmark HSI datasets indicated that the SPaCR, without any preprocessing and postprocessing, outperforms well-known and state-of-the-art classifiers on the limited labeled samples.

## REFERENCES

- [1] B. Tu, C. Zhou, X. Liao, G. Zhang, and Y. Peng, "Spectral-spatial hyperspectral classification via structural-kernel collaborative representation," *IEEE Geosci. Remote Sens. Lett.*, vol. 18, no. 5, pp. 861–865, May 2021.
- [2] A. Sellami, A. B. Abbes, V. Barra, and I. R. Farah, "Fused 3-D spectral-spatial deep neural networks and spectral clustering for hyperspectral image classification," *Pattern Recognit. Lett.*, vol. 138, pp. 594–600, Oct. 2020.
- [3] W. Li, E. W. Tramel, S. Prasad, and J. E. Fowler, "Nearest regularized subspace for hyperspectral classification," *IEEE Trans. Geosci. Remote Sens.*, vol. 52, no. 1, pp. 477–489, Jan. 2014.
- [4] W. Li and Q. Du, "Joint within-class collaborative representation for hyperspectral image classification," *IEEE J. Sel. Topics Appl. Earth Observ. Remote Sens.*, vol. 7, no. 6, pp. 2200–2208, Jun. 2014.
- [5] W. Li, Q. Du, and M. Xiong, "Kernel collaborative representation with Tikhonov regularization for hyperspectral image classification," *IEEE Geosci. Remote Sens. Lett.*, vol. 12, no. 1, pp. 48–52, Jan. 2015.
- [6] Y. Ma, C. Li, H. Li, X. Mei, and J. Ma, "Hyperspectral image classification with discriminative kernel collaborative representation and Tikhonov regularization," *IEEE Geosci. Remote Sens. Lett.*, vol. 15, no. 4, pp. 587–591, Apr. 2018.
- [7] J. Jiang, C. Chen, Y. Yu, X. Jiang, and J. Ma, "Spatial-aware collaborative representation for hyperspectral remote sensing image classification," *IEEE Geosci. Remote Sens. Lett.*, vol. 14, no. 3, pp. 404–408, Mar. 2017.
- [8] W. Li, Y. Zhang, N. Liu, Q. Du, and R. Tao, "Structure-aware collaborative representation for hyperspectral image classification," *IEEE Trans. Geosci. Remote Sens.*, vol. 57, no. 9, pp. 7246–7261, Sep. 2019.
- [9] A. C. Karaca, "Domain transform filter and spatial-aware collaborative representation for hyperspectral image classification using few labeled samples," *IEEE Geosci. Remote Sens. Lett.*, early access, Jun. 16, 2020, doi: 10.1109/LGRS.2020.2998605.
- [10] R. Achanta, A. Shaji, K. Smith, A. Lucchi, P. Fua, and S. Süsstrunk, "Slic superpixels compared to state-of-the-art superpixel methods," *IEEE Trans. Pattern Anal. Mach. Intell.*, vol. 34, no. 11, pp. 2274–2281, Nov. 2012.
- [11] M.-Y. Liu, O. Tuzel, S. Ramalingam, and R. Chellappa, "Entropy-rate clustering: Cluster analysis via maximizing a submodular function subject to a matroid constraint," *IEEE Trans. Pattern Anal. Mach. Intell.*, vol. 36, no. 1, pp. 99–112, Jan. 2014.
- [12] X. Wang, Y. Zhong, L. Zhang, and Y. Xu, "Spatial group sparsity regularized nonnegative matrix factorization for hyperspectral unmixing," *IEEE Trans. Geosci. Remote Sens.*, vol. 55, no. 11, pp. 6287–6304, Nov. 2017.
- [13] F. Melgani and L. Bruzzone, "Classification of hyperspectral remote sensing images with support vector machines," *IEEE Trans. Geosci. Remote Sens.*, vol. 42, no. 8, pp. 1778–1790, Aug. 2004.
- [14] G.-B. Huang, H. Zhou, X. Ding, and R. Zhang, "Extreme learning machine for regression and multiclass classification," *IEEE Trans. Syst., Man, Cybern., B, Cybern.*, vol. 42, no. 2, pp. 513–529, Apr. 2012.
- [15] J. Wright, A. Y. Yang, A. Ganesh, S. S. Sastry, and Y. Ma, "Robust face recognition via sparse representation," *IEEE Trans. Pattern Anal. Mach. Intell.*, vol. 31, no. 2, pp. 210–227, Feb. 2009, doi: 10.1109/TPAMI.2008.79.